Construction and Building Materials 333 (2022) 127445

Contents lists available at ScienceDirect

Construction and Building Materials

journal homepage: www.elsevier.com/locate/conbuildmat

Mechanical, absorptive and freeze–thaw properties of pervious concrete applying a bimodal aggregate packing model

Fan Wu [a,b], Qingliang Yu [b,c,*], H.J.H. Brouwers [b]

[a] Key Laboratory of Mountain Hazards and Earth Surface Process, Institute of Mountain Hazards and Environment, Chinese Academy of Sciences, Chengdu 610041, PR China
[b] Department of the Built Environment, Eindhoven University of Technology, P.O. Box 513, 5600 MB Eindhoven, the Netherlands
[c] School of Civil Engineering, Wuhan University, Wuhan 430072, PR China

ARTICLE INFO

Keywords:
Steel slag
Two-sized aggregate structure
Pervious concrete
Adsorptive aggregate
Phosphorus removal

ABSTRACT

To optimize the pore skeleton structure of pervious concrete to enhance its phosphorus (P) removal from stormwater, small-sized adsorptive aggregate (1–2 mm steel slag) and large-sized natural aggregate (2–5 mm basalt), are applied for the manufacture of two-sized aggregate pervious concrete. Physico-mechanical properties, adsorption performance and freeze–thaw resistance are investigated. The results show that the small-sized steel slag aggregate fills the pores between the large-sized natural aggregates and reduces the porosity and permeability of pervious concrete, significantly improving the mechanical strength and freeze–thaw resistance. The pervious concrete in this study shows an excellent P-adsorption capacity, all P is removed from the aqueous solution with an initial concentration of 168 mg/L and 307 mg/L. The harmful elements (Cr, Sr and V, etc.) leached from the concrete are lower than the maximum limit value. The orthogonal results show that cement and steel slag are the main factors affecting the P-adsorption performance of pervious concrete. Based on the current results, sample 3 (cement: 350 kg/m^3, sand: 500 kg/m^3, W/C: 0.37, 1–2 mm steel slag: 1385.8 kg/m^3 and 2–5 mm basalt: 361.3 kg/m^3) shows good P-removal capacity, which is an optimal mix for pervious concrete to remove P from stormwater, with suitable strength and durability.

1. Introduction

Conventional pervious concrete is typically composed of single-sized coarse aggregates, cement and water or a small amount of fine aggregate [1], which has many advantages, including good drainage properties, noise absorption and urban heat island reduction [2,3]. In recent years, for removing pollutants from stormwater runoff, such as phosphorus (P), nitrogen (N), heavy metals and organic matter, etc., more and more attention has been paid to the adsorption performance of pervious concrete. For example, the expanded shale aggregate is used for permeable pavement for the P and N removal [4]. Besides, pervious concrete is applied to remove heavy metals, such as zine, lead [5,6] and cesium [7] and excess nutrients in the water body [8]. Among these pollutants, P is one of the common pollutants from stormwater runoff and is also the main component causing algal blooms and eutrophication [9,10]. It is important to reduce P from stormwater runoff for a good aqueous environment [11]. However, single-sized aggregates without adsorption capacity are currently the primary aggregates for conventional pervious concrete, consequently, the adsorption capacity and removal rate of conventional pervious concrete is low and usually requires a long reaction time. Therefore, it is hypothetically to improve the P-removal performance of pervious concrete by using materials with adsorption capacity as aggregates and optimizing the micropores of the skeleton structure between the aggregates.

The behavior of concrete is highly related to the aggregate characteristics [12]. The adsorptive materials have been applied to conventional pervious concrete to improve the pollutants removal from stormwater recently. Liang et al. [13] reported that nano-titanium dioxide (TiO_2) is used in pervious concrete to improve the purification efficiency of pollutants (N, P and methylene blue), with an efficiency of 60%-90%. Teymouri et al. [14] investigated the use of 0.6–1.2 mm mineral adsorbents (zeolite and pumice) to improve the compressive strength of pervious concrete and decrease the suspended solids by 40%. Chen et al. [15] studied red mud in geopolymer pervious concrete for heavy metal removal with a removal rate of 53–77% because the geopolymeric gel and red mud have good adsorption for heavy metals,

* Corresponding author at: Department of the Built Environment, Eindhoven University of Technology, P.O. Box 513, 5600 MB Eindhoven, the Netherlands.
E-mail address: q.yu@bwk.tue.nl (Q. Yu).

https://doi.org/10.1016/j.conbuildmat.2022.127445
Received 21 January 2022; Received in revised form 5 April 2022; Accepted 7 April 2022
Available online 11 April 2022

but red mud shows a negative effect on mechanical strength. In addition, a bio-based material, biochar is also added to pervious concrete for N and P removal [16]. Therefore, it is of significance to choose an adsorptive material with appropriate strength and adsorption capacity to improve the adsorption performance of pervious concrete.

Steel slag is the main metallurgical by-product during the steel-making process [17], which contains high contents of CaO, SiO_2 and a small amount of Al_2O_3, Fe_2O_3, etc. [18]. Steel slag accounts for 10–15% of crude steel production depending on the processing methods and the global output of steel slag is 190–280 million tons in 2019 [19]. The main mineral components of steel slag are C_3S, C_2S, C_4AF, C_2F, RO phase (CaO-FeO-MnO-MgO solid solution) and free-CaO, which endows steel slag with cementitious characteristics [20]. Currently, steel slag has been used as aggregates owing to its excellent hardness [17,21,22], and as raw materials of cement due to the high content of mineral components [23,24]. Furthermore, the metallic oxide (CaO and MgO) from steel slag can be applied to capture and store carbon dioxide (CO_2) [25], and steel slag is also used to construct wetlands for P-removal from wastewater [26].

The adsorption mechanism of steel slag on P-solution has been extensively investigated in recent years. The K^+, Na^+ and Mg^{2+} ions released from steel slag have no obvious influence on the P-adsorption capacity, while the Ca^{2+}, $Fe^{2+/3+}$, Al^{3+} ions have a strong affinity with phosphate [27,28]. The relative sequence of the binding capacity of cations on phosphate is: $Ca^{2+} > Mg^{2+} > K^+ > Na^+$ [29]. The main principle is that Ca^{2+} ions released from the steel slag react with the phosphate in the P-solution to form Ca-P precipitates on the steel slag surface. Therefore, steel slag can be applied to replace conventional natural aggregates to enhance the P-removal capacity of pervious concrete.

The main purpose of this study is to improve the P-adsorption and purification function of pervious concrete. In this study, steel slag is applied as adsorptive aggregates to replace conventional aggregates, a two-sized aggregate structure is firstly proposed for improving the adsorption performance, mechanical properties and durability of pervious concrete, and then the effects of cement, sand, water-cement ratio (W/C) and steel slag content on adsorption performance are investigated based on the orthogonal test results. The present work resulted in an optimal mix design of two-sized aggregate pervious concrete with excellent adsorption capacity together with desired mechanical properties and durability for engineering applications.

2. Two-sized aggregate structure for pollutants removal

Natural aggregates are assumed to be spherical, the structure comparison of conventional pervious concrete and two-sized aggregate pervious concrete is shown in Fig. 1. Conventional pervious concrete often contains a single-sized aggregate for high permeability and good anti-clogging properties [30]. However, for two-sized aggregate pervious concrete, low permeability is desirable as long as the pollutants can penetrate the concrete matrix with water flow and be absorbed by adsorptive ingredients. Besides, the low void can lead to an improvement of the mechanical properties [31,32]. Therefore, the two-sized aggregate structure is applied to improve the adsorption and purification function of pervious concrete in this study. Natural aggregates with larger particle sizes are used as the skeleton, and the adsorptive particles with smaller size ranges are filled into the skeleton voids as the main body for pollutants removal by physical and chemical adsorption. The large-sized natural aggregates and small-sized adsorptive aggregates form a two-sized structure. Furthermore, the large-sized aggregates can also be replaced with adsorptive aggregates to further improve the adsorption capacity of pervious concrete.

The mathematical relationship of the particle size between the natural aggregate and the adsorptive aggregate is shown in Fig. 2. The optimized particle packing can enhance the mechanical properties and durability of pervious concrete [33,34]. When the natural aggregate is single-sized, usually two arrangements (triangular array and square array) exist between aggregates from a two-dimensional perspective. There are three types of holes formed by two arrangements, including cube pore, octahedral pore and tetrahedral pore (Fig. 2) [35]. For example, when using natural aggregates as a skeleton with a particle size of $R_1 = 5$ mm, the maximum particle size of the adsorptive aggregate is $R_2 = 1.15$ mm, 2.05 mm or 3.65 mm based on three packing modes. When the particle size of the natural aggregate is selected as 5 mm, the adsorptive aggregate size should not exceed 2.05 mm to make small-sized adsorptive aggregate smoothly fill the pore structure for a good micropore structure of pervious concrete. The small-sized adsorptive aggregate can fit into these holes, theoretically, the particle size range of the adsorptive aggregate can be estimated for good packing modes using:

$$\boldsymbol{R}_2 = \left(\sqrt{3} - 1\right)\boldsymbol{R}_1 \tag{1}$$

$$\boldsymbol{R}_2 = \left(\sqrt{2} - 1\right)\boldsymbol{R}_1 \tag{2}$$

$$\boldsymbol{R}_2 = \left(\frac{\sqrt{6}}{2} - 1\right)\boldsymbol{R}_1 \tag{3}$$

The mechanical strength of pervious concrete can be significantly improved by using two-sized aggregates. Previous studies show that pervious concrete made from small-sized aggregates (5–10 mm) shows 1.8–2 times higher strength than those with large-sized aggregates (10–20 mm) [36]. The appropriate proportioning of aggregates combined with different particle sizes results in a 156% increase in strength thanks to the packing optimization [34]. The two-sized aggregate concrete (mixing 50% fine aggregates and 50% coarse aggregates) results in

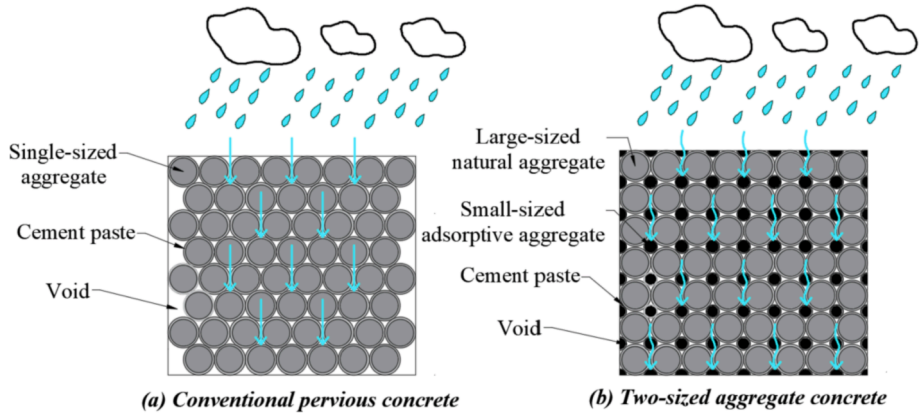

Fig. 1. Structure comparison of conventional pervious concrete and two-sized aggregate pervious concrete.

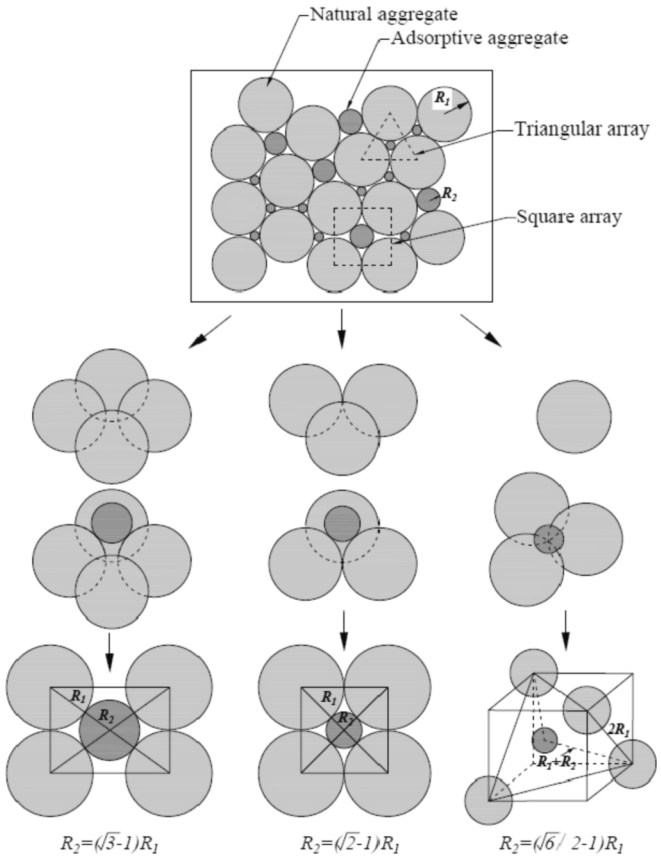

Fig. 2. Three packing forms of two-sized aggregates (R_1: natural aggregate size; R_2: adsorptive aggregate size).

the maximum packing density studied by Sebaibi et al. [37]. Klein et al. [38] found that the minimum void index is obtained when the fine aggregates account for 60% of the two-sized aggregates by mass. Dai et al. [39] reported the addition of admixture is more effective to improve the mechanical strength of pervious concrete than to increase fine aggregate content. Under the premise of ensuring that the stormwater can penetrate micropores of pervious concrete, the optimization of the micropores can also improve the durability of pervious concrete such as freeze–thaw resistance for long service life.

This study aims to improve the adsorption performance, mechanical properties and durability of pervious concrete. The experiment in this study consists of two main parts. In the first part, the small-sized steel slag (1–2 mm) is used as adsorptive aggregate to replace the large-sized basalt (2–5 mm) based on the adsorptive aggregate results in our previous work [11], the effects of the steel slag substitution ratio by volume from 0% to 50% (increments of 12.5%) on the physical–mechanical properties, P-adsorption performance and freeze–thaw resistance of pervious concrete are investigated. In the second part, the effects of cement, sand, W/C and steel slag on the mechanical strength, multiple adsorption cycles and durability of pervious concrete are evaluated through an orthogonal test, and the optimum mix ratio of two-sized aggregate pervious concrete is obtained.

3. Materials and methods

3.1. Materials

The basalt with a particle size of 2–5 mm is used as coarse aggregates. The converter steel slag (TATA Steel, The Netherlands) with 1–2 mm particle size is used as an alternative for the fine aggregates (Fig. 3). The specific densities of the basalt and the steel slag are 3.05 g/cm^3 and 3.9 g/cm^3, respectively. The microscopic image of the steel slag shows a dense microstructure (Fig. 4a). The chemical composition of the steel slag is analyzed by X-ray fluorescence (XRF), and the steel slag is mainly composed of metal oxides, including CaO, Fe_2O_3, SiO_2 and MgO, as shown in Table 1. The main mineral components of the steel slag are $3CaO{\cdot}SiO_2$ (C_3S), $2CaO{\cdot}SiO_2$ (C_2S) and RO (Fe_2O_3, MgO and MnO) based on the X-ray diffraction (XRD) analysis (Fig. 4b). Portland cement CEM I 52.5 R (ENCI, The Netherlands) is used as the binder. CEN-NORM sand satisfied with European standards (EN 196–1) is used as fine aggregates.

3.2. Mix proportion and specimen preparation

3.2.1. Effects of the steel slag on the performance of pervious concrete

Firstly, the effects of the small-sized steel slag on the physical and mechanical properties, adsorption performance and freeze–thaw resistance of pervious concrete are evaluated. A mixture containing 301 kg/m^3 cement, 110 kg/m^3 sand, 111.4 kg/m^3 water and 1574 kg/m^3 basalt is used as the control mix, which refers to the mix proportion of pervious concrete as reported by Nguyen et al [41]. The 2–5 mm basalt is replaced by 1–2 mm steel slag to form a two-sized skeleton structure in the other four batches, and other parameters are kept constant. The alternative volume ratios are set as 12.5%, 25%, 37.5% and 50%, respectively. The mix proportions of pervious concrete are presented in Table 2.

3.2.2. Mix proportion of orthogonal test

The orthogonal test is used to investigate the optimal mixing ratio of two-sized aggregate pervious concrete. The effects of four factors (including cement, sand, W/C and the volumetric content of steel slag in total aggregates) on physical and mechanical properties, adsorption

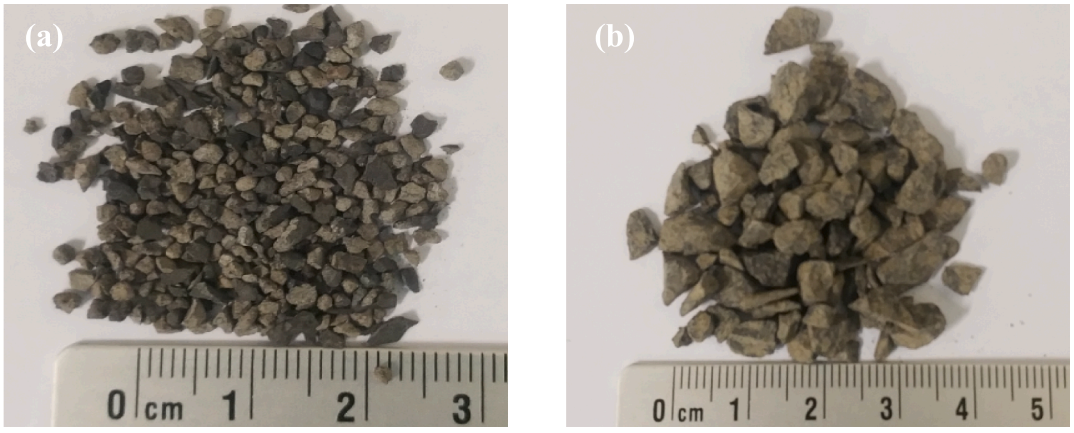

Fig. 3. (a) Steel slag and (b) Basalt.

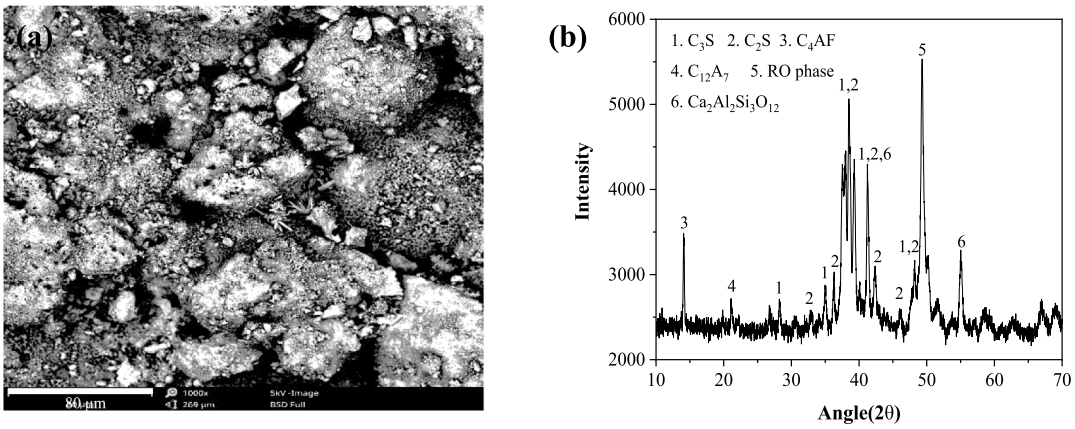

Fig. 4. (a) Microscopic images and (b) X-ray diffraction of steel slag.

Table 1
Chemical composition of steel slag and cement (wt.%) [40].

Oxides	CaO	SiO_2	Al_2O_3	Fe_2O_3	SO_3	MgO	K_2O	Na_2O	LOI
Steel slag	37.97	10.37	1.61	31.48	0.43	4.92	–	–	0.72
Cement	64.60	20.08	4.98	3.24	3.13	1.98	0.53	0.27	0.40

Table 2
Mix proportions of pervious concrete.

Samples	Cement (kg/m^3)	Sand (kg/m^3)	Water (kg/m^3)	Aggregates		Steel slag /total aggregates (Vol.%)
				1–2 mm Steel slag (kg/m^3)	2–5 mm Basalt (kg/m^3)	
Control	301	110	111.4	0	1574	0
SS12.5	301	110	111.4	251.58	1377.25	12.5
SS25	301	110	111.4	503.16	1180.5	25
SS37.5	301	110	111.4	754.74	983.75	37.5
SS50	301	110	111.4	1006.32	787	50

performance and freeze–thaw resistance of pervious concrete are investigated, and each factor is designed as three levels, as shown in Table 3. The orthogonal table L9(3^4) is applied in the orthogonal test, the mix proportions of pervious concrete are shown in Table 4.

3.3. Test methods

3.3.1. Physical and mechanical properties

The density of the sample is measured following EN 12390-7. The porosity of the samples is determined according to ASTM C1754/C1754M-12. The cross-section of the sample after the flexural test is captured by a high-resolution camera for evaluation of internal pore properties including pore area fraction and average pore size, etc. based on the image analysis method by the Image J software [42]. A random location of 40 × 40 mm^2 on the casting surface of the sample is used as the surface pore analysis. Considering the apparent differences in the casting surface of the sample, the change in porosity of the entire casting surface along with the length of the sample is analyzed.

Table 3
Factors and levels of the orthogonal test.

Three levels	Four factors			
	Cement (kg/m^3)	Sand (kg/m^3)	W/C	1–2 mm steel slag/ total aggregate (Vol.%)
1	350	400	0.33	25
2	400	450	0.35	50
3	450	500	0.37	75

The 28-day compressive strength and flexural strength of the sample are determined according to EN 196-1. Fragments of the sample are collected after the compression test for microstructure analysis using a scanning electron microscope (SEM).

The porosity can be calculated according to:

$$\boldsymbol{P} = [1 - (\frac{\mathbf{M}_{dry} - \mathbf{M}_{sub}}{\boldsymbol{\rho}_{water} \times \boldsymbol{V}_s})] \quad (4)$$

where P is the total porosity of the sample (%); M_{dry} is the dry mass of the sample (kg); M_{sub} is the submerged mass of the sample in water (kg); V_s is the volume of the sample (m^3); ρ_{water} is the density of water (kg/m^3).

The water permeability of the sample is determined using the falling head method, and the coefficient of water permeability is calculated based on Darcy's Law as shown by:

$$\boldsymbol{k} = \frac{\boldsymbol{a} \times \boldsymbol{L}}{\boldsymbol{A} \times \boldsymbol{t}} \boldsymbol{ln}\left(\frac{\boldsymbol{h}_1}{\boldsymbol{h}_2}\right) \quad (5)$$

where k is the water permeability coefficient (mm/s); a is the cross-sectional area of pipe (mm^2); A is the cross-sectional area of the cylindrical sample (mm^2); L is the length of the sample (mm); t is the time when the water head varies from h_1 to h_2; $h_1$is the initial water head (mm); h_2 is the final water head (mm).

3.3.2. Adsorption performance

The adsorption performance of pervious concrete is evaluated by the P-solution removal test in this study. Considering the high P-removal performance of steel slag aggregates [11], four initial concentrations of P-solution, including low-concentration (168 mg/L and 307 mg/L) and high-concentration (1869 mg/L and 2898 mg/L) are prepared for the P-adsorption test by dissolving the chemically pure potassium dihydrogen phosphorus (KH_2PO_4) in distilled water. After that, the P-solution is stirred at 225 rpm in a thermostatic shaker for 24 h for the dissolution of the solid P-particle before the adsorption test.

The P-adsorption test of pervious concrete in this study refers to the laboratory setup method for the removal of stormwater pollutants reported by Haselbach et al. [43], as shown in Fig. 5. The 40 × 40 × 160 mm^3 sample is cut into a small cube block (approximately 4 × 4 × 4.5 mm^3) for the P-adsorption test. Firstly, 100 ml of P-solution is poured into a glass container, and then the control valve is opened, the P-

Table 4
Mix proportions of the orthogonal test.

Samples No.	Cement (kg/m^3)	Sand (kg/m^3)	W/C	Water (kg/m^3)	Aggregates			
					1–2 mm Steel slag (kg/m^3)	Steel slag /total aggregate (Vol. %)	2–5 mm Basalt (kg/m^3)	Basalt/total aggregate (Vol. %)
1	350	400	0.33	115.5	511.4	25	1199.9	75
2	350	450	0.35	122.5	973.4	50	761.2	50
3	350	500	0.37	129.5	1385.8	75	361.3	25
4	400	400	0.35	140	1415.4	75	369.0	25
5	400	450	0.37	148	446.1	25	1046.6	75
6	400	500	0.33	132	887.5	50	694.1	50
7	450	400	0.37	166.5	860.5	50	673.0	50
8	450	450	0.33	148.5	1289.6	75	336.2	25
9	450	500	0.35	157.5	403.2	25	945.9	75

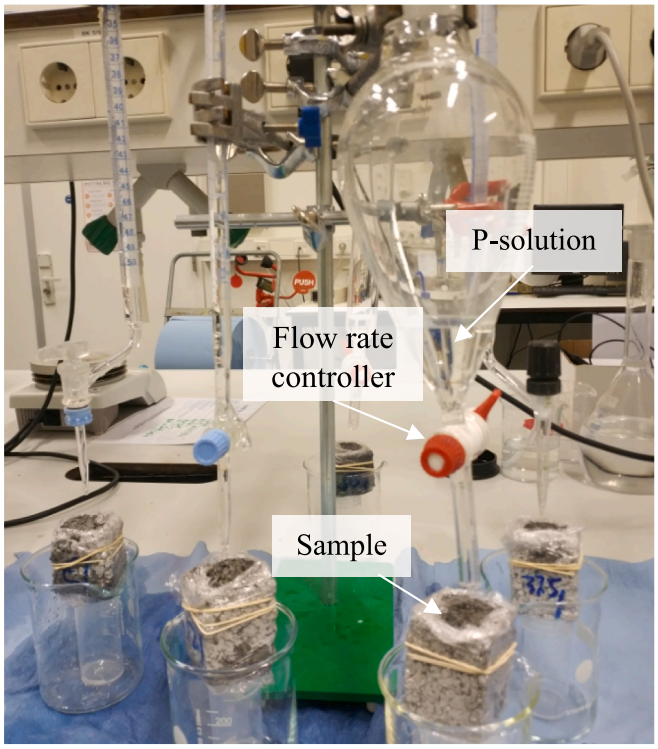

Fig. 5. Laboratory setup for P-removal test.

solution is slowly dripped onto the surface of the concrete block with a flow rate of 3–5 ml/min, a beaker at the bottom is used to collect the filtrate. When the P-solution is completely filtered by the concrete block, the collected filtrate is immediately poured into the upper glass container to continue the next cyclic P-adsorption test. After P-solution is adsorbed by the concrete block for 1, 3 and 5 times, about 3 ml of filtrate is collected by an injecter and then filtered by a 0.45 μm membrane filter and the P-concentration of the filtrate is determined using an ion chromatography (IC) analyzer. The mass of the small cube block for the cyclic adsorption test is shown in Table 5.

The P-adsorption capacity (q, mg/g) and P-removal rate (P_R, %) are calculated according to Eqs. (5) and (6), respectively. The harmful metal ions such as Cr, Sr and V, etc. released from pervious concrete is determined according to EN 12457-2 through inductively coupled plasma atomic emission spectroscopy (ICP-AES), and the environmental impact of pervious concrete is analyzed:

$$\mathbf{q} = \frac{\boldsymbol{C_0} - \boldsymbol{C_e}}{\boldsymbol{M}} \times \boldsymbol{V} \tag{6}$$

$$\boldsymbol{P_R} = \frac{\boldsymbol{C_0} - \boldsymbol{C_e}}{\boldsymbol{C_0}} \times 100\% \tag{7}$$

where C_0 is the initial P-concentration (mg/L), C_e is the P-concentration in the solution at equilibrium (mg/L), M is the mass of sample (g), and V is the volume of solution (L).

3.3.3. Freeze-thaw test

The freeze–thaw resistance of pervious concrete is an important durability indicator when it is applied in cold regions. The resistance to freeze–thaw cycles of pervious concrete is evaluated according to EN 1338. The temperature of the freeze–thaw test varies from −18 °C to 20 °C for 24 h. The prism samples of 40 × 40 × 160 mm^3 are completely immersed in the water, and the water surface is 5 ± 2 mm above the surface of the sample. The mass loss and apparent change of the sample after each freeze–thaw cycle is evaluated.

4. Results and discussion

4.1. Effects of steel slag on performance of pervious concrete

4.1.1. Density, porosity and permeability

Generally, the aggregate size and shape have a significant effect on the porosity and permeability of pervious concrete [12,44]. As shown in Fig. 6, the replacement of basalt aggregate with small-sized steel slag aggregate increases the density of pervious concrete and reduces the porosity and permeability coefficient. When 50% basalt (2–5 mm) is replaced by 1–2 mm steel slag, the density of pervious concrete increases by 26.4% and the porosity and permeability coefficient reduce by 35.7% and 63.4%, respectively. The phenomenon of smaller aggregate size leads to a lower permeability of pervious concrete is reported in previous studies [45]. The tendency of an increase in pore sizes of pervious concrete with the increase of aggregate particle sizes can be easily noticed [42].

The pores have a relatively uniform distribution as the pores are smaller and regular [46]. In this study, the pores of the SS50 concrete are more uniform than that of the control concrete. Besides, the small-sized

Table 5
Mass of the small cube block for cyclic adsorption test.

P-concentration (mg/L)	Sample mass (g)								
	1	2	3	4	5	6	7	8	9
1869	144	146.5	140	150.6	144.2	153.7	168.8	167.4	176.3
2898	152.5	153.5	148.3	156.2	137.2	159.3	170.8	166.8	178.8

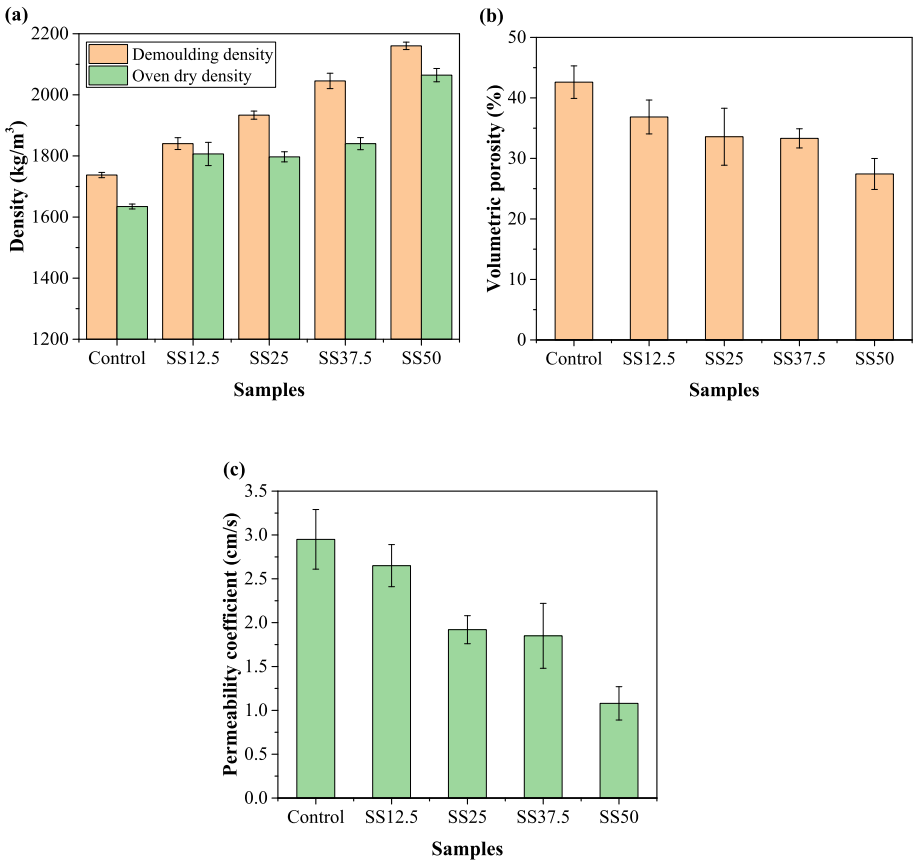

Fig. 6. Density, volumetric porosity and permeability coefficient of pervious concrete.

steel slag fills the large pores between aggregates, resulting in a significant decrease in porosity. The mechanical strength and permeability of pervious concrete mainly depend on micropores, cement paste and aggregate characteristics [47]. The reduced porosity through the small-sized aggregate can contribute to the strength enhancement of pervious concrete.

4.1.2. *Compressive strength and flexural strength*

The relationship between 28-day mechanical strength and porosity of pervious concrete is shown in Fig. 7. The results show that as the content of small-sized steel slag increases, the 28-day compressive strength and flexural strength of pervious concrete gradually increase. When the coarse aggregate is replaced by 50% steel slag, the compressive strength and flexural strength are 14.3 MPa and 5.19 MPa, respectively, with an increase of 150.8% and 130.7%, compared to the control concrete. This may be attributed to the good packing density [37], low porosity and particle interlock formed by the two-sized aggregates [38]. It can be concluded that the mixing of 1–2 mm steel slag aggregate and 2–5 mm natural aggregate results in an increased aggregate packing density, contributing to the improvement of the mechanical strength.

Generally, the interfacial transition zone is the weakest part of conventional concrete, which dominates the performance of the concrete [48]. However, the designed porosity is the weakest part of pervious concrete. In this study, small-sized steel slag fills the pores between the aggregates and decreases the porosity of pervious concrete, thus

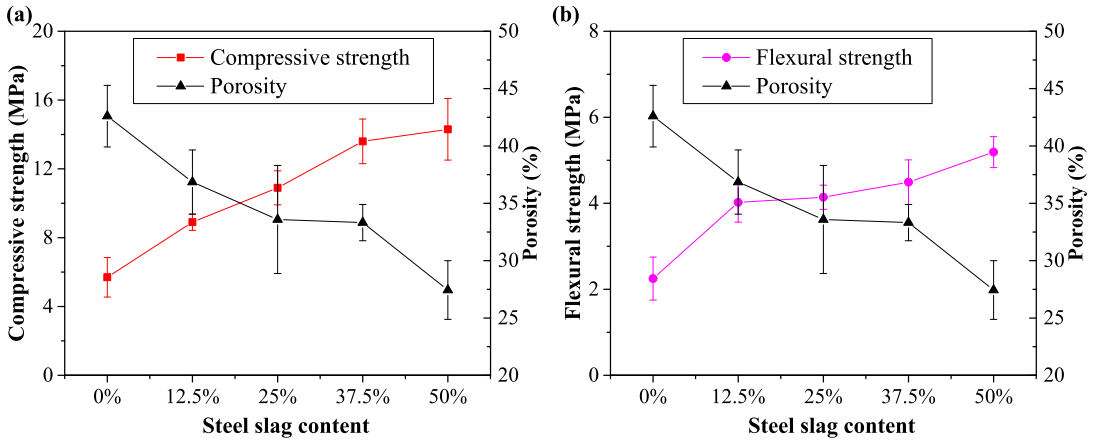

Fig. 7. Relationship between 28-day compressive strength and flexural strength and porosity of pervious concrete.

improving the mechanical strength. Moreover, steel slag has a higher density and strength than basalt aggregate. The application of the high strength waste aggregates (e.g. copper slag [12], steel slag [49], etc.) can enhance the mechanical strength due to the strong interlocking effect [48]. The use of cement, fine aggregates, polymeric materials, fibres, etc. will further improve the mechanical properties of pervious concrete [50–53].

The microscope images of the interfacial transition zone (ITZ) of pervious concrete are shown in Fig. 8. A good bond between basalt and mortar is observed, however, a small number of microcracks is produced between the ITZ and the surface of basalt aggregate during the compression test (Fig. 8a). The micro-cracks are observed in the ITZ between steel slag and mortar, but no steel slag cracking (Fig. 8b), indicating that the ITZ between steel slag and mortar is the weakest part of pervious concrete, which needs to be strengthened in future work.

4.1.3. P-adsorption performance

The initial concentration of the P-solution is 168 mg/L and 307 mg/L, respectively. The results show that no P is detected in the filtrate, indicating that all P in the solution is adsorbed by pervious concrete. This may be attributed to the calcium ions (Ca^{2+}) and hydroxide ions (OH^{-}) released from the pervious concrete reacting with the phosphate to form Ca-P precipitates on the pervious concrete surface [54,55]. Moreover, when pervious concrete is immersed in water for a long time, the aquatic microbes attached to the porous structures also contribute to the biological adsorption [36], and the internal micropores have physical adsorption for the suspended substances from stormwater [56]. Therefore, the P-removal performance of pervious concrete depends on the connected pore structure of pervious concrete, in addition to the adsorption capacity of the adsorptive aggregate and the mortar matrix.

The comparison of pollutant removal of different concretes from stormwater runoff is shown in Fig. 9. For conventional concrete, stormwater containing pollutants can not penetrate the conventional concrete, only the surface contacts with pollutants, and the pollutant removal of the conventional concrete can be ignored (Fig. 9a). During the infiltration of stormwater into the pervious concrete, the ions (calcium, iron, aluminium and hydroxide ions, etc.) leached from the cement paste of pervious concrete can adsorb a small amount of pollutants (methylene blue, phosphorus, nitrogen and heavy metals, etc.) through surface complexation, ion exchange and precipitation [13,57]. The conventional single-sized pervious concrete exhibits a certain adsorption capacity for pollutants (Fig. 9b), however, it usually has a low adsorption capacity and a long contact time [11]. Due to the high adsorption capacity of the adsorptive aggregate, more pollutants can be combined with the adsorptive aggregate and cement matrix, significantly improving the pollutant removal capacity of pervious concrete by a two-sized aggregate structure (Fig. 9c). Moreover, when the large-sized natural aggregate is completely replaced by the adsorptive aggregates, the adsorption capacity of pervious concrete would be further improved.

During the rainy season, the stormwater penetrates into the voids of pervious concrete, which then dissolves the hydration products of cement paste [58]. The dissolved ions are then washed out from pervious concrete by stormwater. Therefore, when steel slag is used as aggregates for pervious concrete, the leaching behavior should be evaluated in this study, and the leaching results are shown in Table 6. The amount of sodium and potassium is 50–100 mg/kg and the calcium ion is above 500 mg/kg. Some harmful metal ions such as As, Cr, V, etc. leached from the steel slag particle and pervious concrete are far below the maximum limit values for building materials according to the Dutch Soil Quality Decree [59]. The results confirm that the pervious concrete produced in this study can be used for P-removal without any environmental risk.

4.1.4. Freeze-thaw resistance

(1) Mass loss

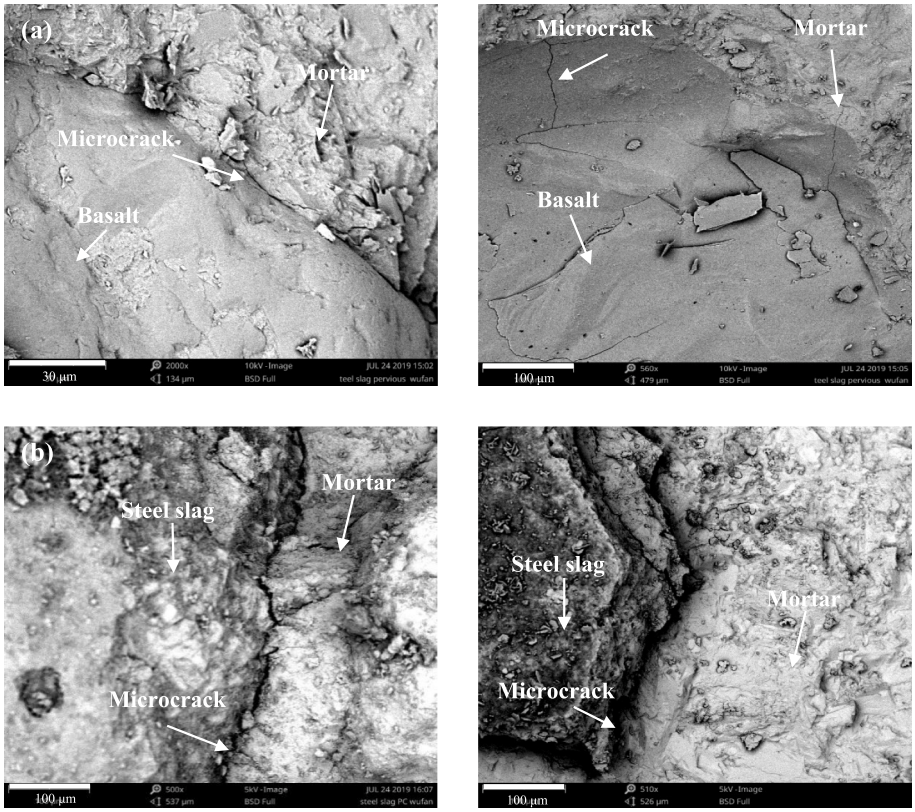

Fig. 8. Microscope images of the ITZ (a) basalt and (b) steel slag.

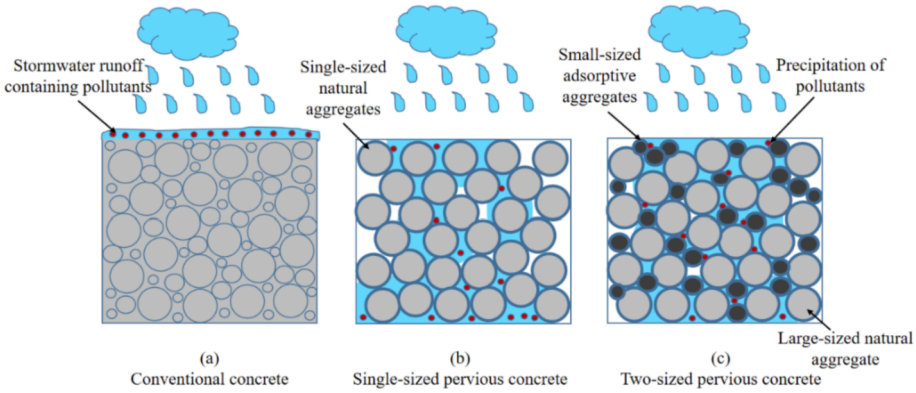

Fig. 9. Comparison of pollutant removal from stormwater runoff by (a) conventional concrete, (b) single-sized pervious concrete and (c) two-sized pervious concrete.

Table 6
Leaching results of steel slag aggregate and two-sized pervious concrete (mg/kg).

Elements	Al	As	Ba	Cr	Fe	Mg	Sr	V
Steel slag	3.492	≤0.18	0.004	0.132	≤0.252	0.548	0.372	≤0.952
Control	1.412	≤0.18	3.436	0.052	≤0.148	0.04	21.18	≤0.216
SS12.5	0.06	≤0.18	3.796	0.052	≤0.224	0.044	21.3	≤0.216
SS25	≤0.016	≤0.18	3.124	0.036	≤0.228	0.04	21.008	≤0.216
SS37.5	≤0.312	≤0.18	3.32	0.052	≤0.224	0.04	21.108	≤0.212
SS50	≤0.276	≤0.18	3.544	0.072	≤0.248	0.024	21.028	≤0.216
Limit value	–	0.90	22	0.63	–	–	–	1.80

Pervious concrete is applied to remove pollutants from stormwater runoff and often in contact with an aqueous solution, the resistance to freeze–thaw cycles of pervious concrete should be evaluated when it is applied in the cold region. As shown in Fig. 10, the SS50 concrete has the best resistance to freeze–thaw cycles, compared to the control concrete. The use of small-sized steel slag instead of basalt significantly improves the freeze–thaw resistance of pervious concrete. After 28 freeze–thaw cycles, the mass loss of the control, SS12.5, SS25, SS37.5 and SS50 concrete are 3.8%, 3.2%, 2.7%, 1.7% and 0.9%, respectively. The mass loss of the SS50 concrete decreases by 73.7%, compared to the control concrete. The spalling of aggregates from the concrete surface may lead to the increase of mass loss, for example, a significant increase in mass loss of the SS12.5 concrete is observed at 21 freeze–thaw cycles. The freeze–thaw characteristics of the pervious concrete can be improved by using a two-sized aggregate structure composed of fine steel slag and normal coarse aggregate.

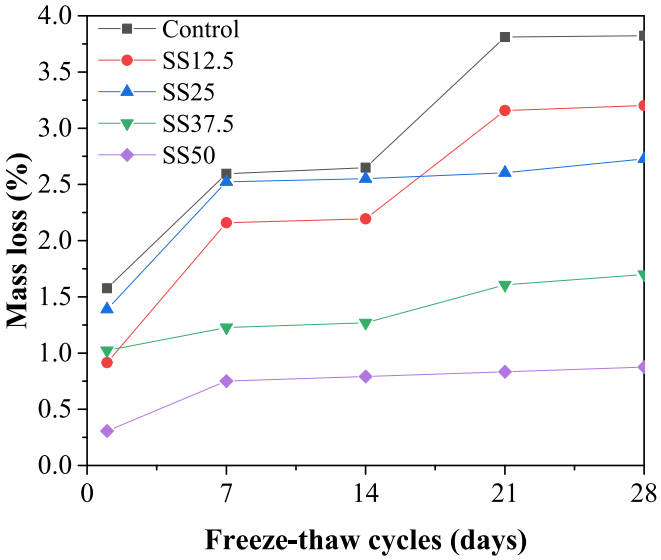

Fig. 10. Mass loss of pervious concrete during the freeze–thaw test.

The main degradation form of freeze–thaw damage is the cracking and spalling of the concrete surface [60,61]. The effects of pore pressures on the micropores of two-sized aggregate pervious concrete during freeze–thaw cycles are illustrated in Fig. 11, the freeze–thaw damage is mainly caused by the pore pressure due to the ice formation [60,62]. The pore pressure is composed of the hydraulic pressure (by the ice volume expansion), cryosuction pressure (by the surface tension of the water) and crystallization pressure (by the shape of ice crystals), depending on thermodynamics between ice crystal and unfrozen water [63–65]. The hydraulic pressure mainly relies on the increased ice volume due to expansion, while the cryosuction pressure and crystallization pressure depend on pore size and temperature [63]. In this study, when the basalt is replaced by small-sized steel slag, the internal defects or micropores of the pervious concrete is reduced, and the hydraulic pressure generated by the ice expansion also significantly decreases, which contribute to the good freeze–thaw resistance of two-sized aggregate pervious concrete.

(2) Strength loss

The effects of freeze–thaw cycles on the mechanical strength of pervious concrete are analyzed, as shown in Table 7. The results show that the compressive strength and flexural strength significantly decrease after freeze–thaw cycles. However, when the basalt is replaced by the small-sized steel slag, the reduction in mechanical strength is rather limited. After 15 freeze–thaw cycles, the reduction in the compressive strength and flexural strength of the SS50 concrete is only 3.5% and 7.3%, respectively, which is significantly lower than the reduction in the strength of the control concrete.

The degrading effect of freeze–thaw cycles on the mechanical properties of concrete has been observed in previous studies [66]. The cracks caused by freeze–thaw damage are the main reasons for strength reduction [67]. According to the degradation model of strength as reported by Sun et al. [66], the relative compressive strength of conventional concrete after 15 freeze–thaw cycles is approximately 0.96, with a compressive strength loss of about 4%. It is noted that SS50 developed in

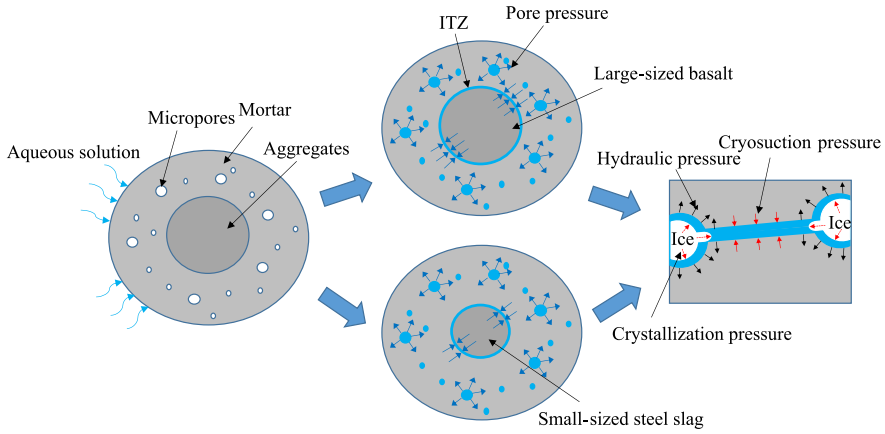

(a) Concrete containing micropores (b) Ice formation in micropores (c) Pore pressure in micropores

Fig. 11. Schematic diagram of the freeze–thaw failure mechanism of two-sized aggregate pervious concrete.

Table 7
Mechanical strength loss of pervious concrete after 15 freeze–thaw cycles.

Samples	Compressive strength (MPa)			Flexural strength (MPa)		
	Before	After	Reduction in %	Before	After	Reduction in %
Control	5.7	4.5	21.1	2.25	2.06	8.4
SS12.5	8.9	8.0	10.1	4.02	3.68	8.5
SS25	10.9	9.5	12.8	4.14	3.64	12.1
SS37.5	13.6	11.0	19.1	4.49	4.32	3.8
SS50	14.3	13.8	3.5	5.19	4.81	7.3

this work show a comparable compressive strength loss with conventional concrete, indicating its excellent durability performance.

4.2. Orthogonal results of two-sized aggregate pervious concrete

In the first section, the small-sized steel slag shows a significant effect on the physical and mechanical properties, P-adsorption performance and freeze–thaw resistance of pervious concrete. The optimum mix ratio of two-sized aggregate pervious concrete containing small-sized steel slag is investigated based on the orthogonal test results in the next section.

4.2.1. Physical properties

The surface texture of pervious concrete is shown in Fig. 12. The results show that samples 2, 3, and 4 have a perfect surface, the small-sized steel slag is tightly embedded between the basalt aggregates, and the overall surface is relatively smooth compared to samples 1 and 5. The surfaces of samples 8 and 9 are covered by mortar, most of the micropores are filled with mortar and the porosity is lower. No micropores are observed on the surface of sample 9 and all micropores are blocked by mortar, which will significantly affect the penetration of pollutants into the pervious concrete and reduce its adsorption performance.

The porosity, water absorption and density of pervious concrete are shown in Table 8. The results show that the area fraction and the average pore size of the surface pore of the most pervious concrete are higher than that of the internal pore. It is noted that the calculated area fraction of surface pores of samples 7, 8, and 9 are very low because these three samples have more cement content (450 kg/m^3), resulting in the blockage of the pores of the concrete by the excessive cement paste, consequently, showing lower water absorption and higher density compared to other sample series. Generally, the target porosity of pervious concrete should be 15–35% considering the requirements of the anti-clogging characteristic [68]. The low-porosity pervious concrete may have a clogging problem, and further research is needed in future work.

The change in porosity of the entire casting surface along with the length of samples 3, 6 and 9 is analyzed by the image analysis method, as shown in Fig. 13. The porosity of the entire casting surface of samples 3, 6 and 9 unevenly distribute along with the length, with a range of

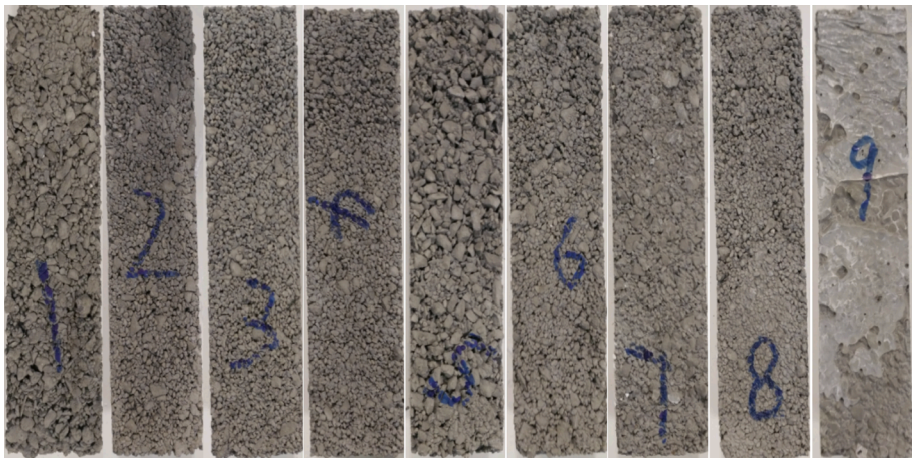

Fig. 12. Surface texture of pervious concrete.

Table 8
Porosity, water absorption and density of pervious concrete.

Samples	Internal pore obtained by image analysis		Surface pore obtained by image analysis		Volumetric porosity obtained by test (%)	24-hour water absorption (%)	Oven-dry density (kg/m^3)
	Area fraction of pores (%)	Average pore size (mm)	Area fraction of pores (%)	Average pore size (mm)			
1	9.6	0.06	11.6	0.06	14.3	6.0	2081
2	9.0	0.04	11.1	0.04	15.8	6.6	2084
3	6.2	0.03	11.1	0.05	17.4	7.3	2013
4	8.9	0.04	16.4	0.07	17.2	7.2	2132
5	1.5	0.03	12.0	0.10	13.2	5.5	2048
6	4.9	0.04	11.6	0.05	13.8	5.5	2198
7	4.1	0.04	3.1	0.02	11.2	4.9	2390
8	9.5	0.02	3.9	0.03	12.3	4.9	2325
9	1.2	0.04	0.1	0.01	9.0	4.0	2484

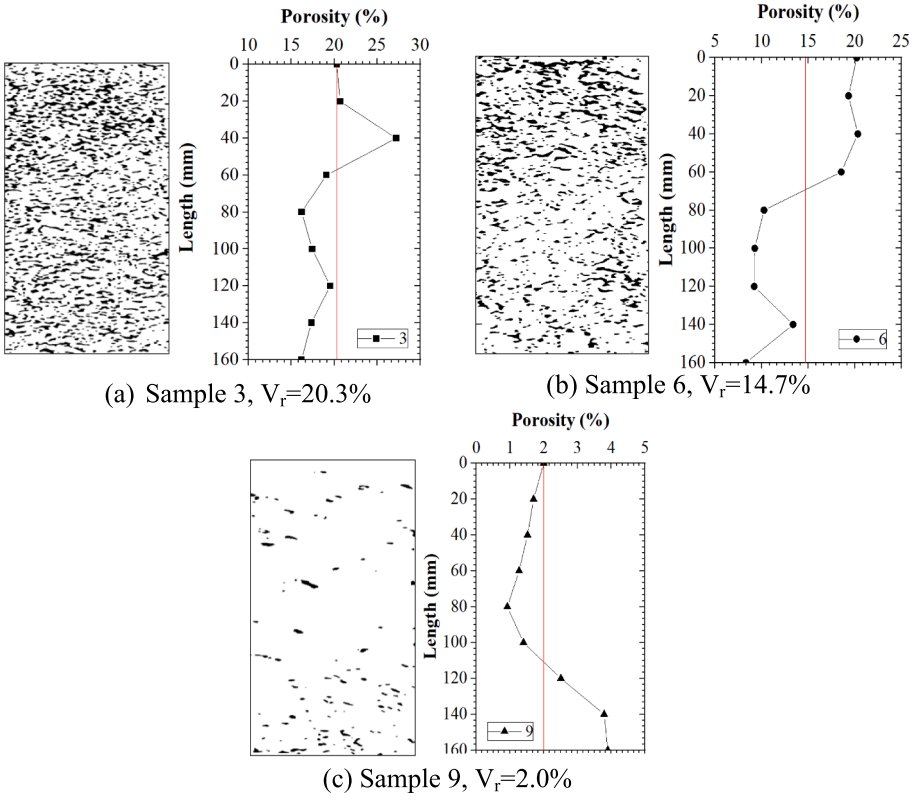

(a) Sample 3, V_r=20.3%
(b) Sample 6, V_r=14.7%
(c) Sample 9, V_r=2.0%

Fig. 13. Changes in porosity of the entire casting surface of pervious concrete with its length (black areas are pores).

16.2–27.2%, 8.3–20.3% and 0.9–3.9%, respectively. In the length range, the average porosity of the entire casting surface of samples 3, 6 and 9 is 20.3%, 14.7% and 2.0%, respectively. The porosity of the entire casting surface of sample 3 more evenly distributes along with the length compared with samples 6 and 9, which is helpful for pollutants removal by pervious concrete.

4.2.2. Mechanical properties

The compressive strength and flexural strength of samples 1, 2, and 3 series with a cement content of 350 kg/m^3, which are significantly different from those of samples 4, 5, and 6 series (cement: 400 kg/m^3) and sample 7, 8, and 9 series (cement: 450 kg/m^3), as shown in Fig. 14. These results are consistent with the porosity results, i.e., samples 1, 2, and 3 series with a high porosity result in a low compressive strength (27.0–31.3 MPa), while samples 7, 8, and 9 series with a low porosity show a higher compressive strength (45.7–71.7 MPa). The compressive strengths of samples 4, 5 and 6 series vary from 31.5 MPa to 39.4 MPa. Similar to the compressive strength, the flexural strength in this study shows a similar trend. The flexural strengths of samples 1–3, 4–6 and 7–9 series vary between 6.21 and 6.25 MPa, 6.91–7.20 MPa and 8.08–8.47 MPa, respectively.

4.2.3. Adsorption performance

(1) P-adsorption capacity and removal rate

Considering the low-concentration P solution (168 mg/L and 307 mg/L) is totally adsorbed by pervious concrete in the first part, a much higher concentration of P solution (1869 mg/L and 2898 mg/L) is applied to the present adsorption test. As shown in Fig. 15, the P-adsorption capacity and P-removal rate of pervious concrete have a significant difference. The P-adsorption capacity and removal rate of samples 1, 2, and 3 series are better than other samples series. When the P-concentration is 1869 mg/L, the P-adsorption capacity of samples 1–3, 4–6 and 7–9 series varies between 0.15 and 0.30 mg/g, 0.06–0.29 mg/g and 0.01–0.04 mg/g, respectively, the corresponding P-removal rates are 11.2–22.2%, 5.2–23.1% and 1.3–3.6%, respectively. The high P-removal rate of samples 1, 2, and 3 series may be attributed to the

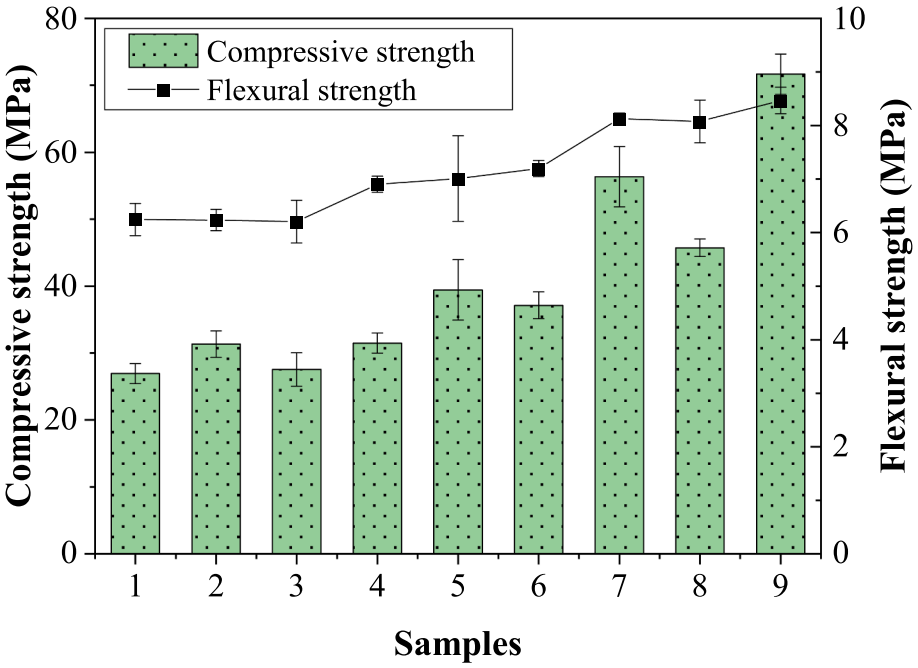

Fig. 14. 28-day compressive strength and flexural strength of pervious concrete.

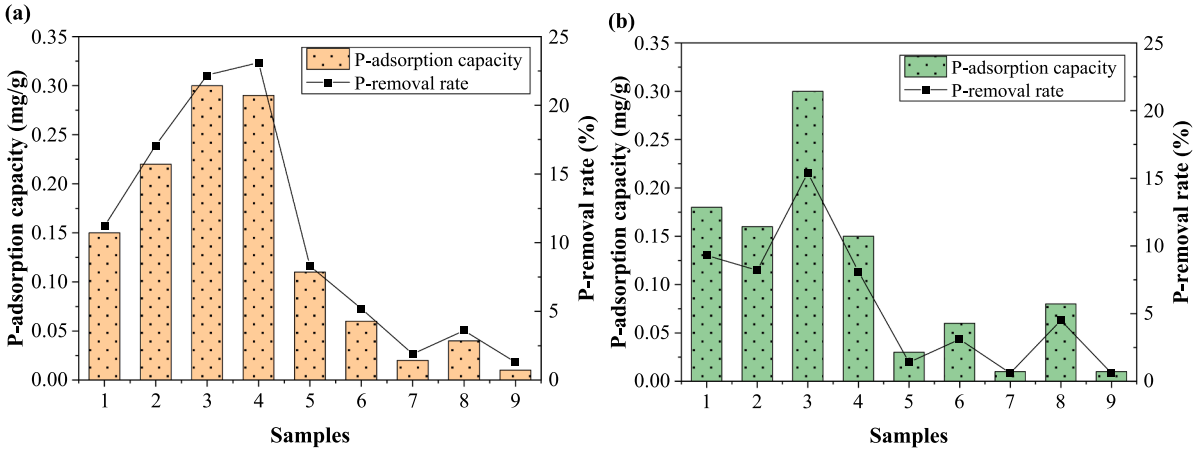

Fig. 15. P-adsorption capacity and removal rate of pervious concrete in P- solution of (a) 1869 mg/L and (b) 2898 mg/L.

relatively high porosity and water absorption, therefore, phosphate in the solution can easily contact calcium ions for Ca-P precipitates. Although samples 7, 8, and 9 series have high mechanical strength, the adsorption capacity is very low, compared to other sample series.

The significance of cement, sand, W/C and small-sized steel slag content on the adsorption capacity are analyzed through the variance analysis. The calculated results are shown in Table 9. The deviation analysis of the orthogonal test results of P-adsorption capacity is calculated based on [69]:

$$K = \sum_{l=1}^{r} K_{jl} \tag{8}$$

$$P = \frac{1}{n} K^2 \tag{9}$$

$$Q = \sum_{i=1}^{n} p_i^2 \tag{10}$$

Table 9
Deviation calculation of the orthogonal results of P-adsorption capacity.

Sample No. (n)	Cement (kg/m^3)	Sand (kg/m^3)	W/C	1–2 mm steel slag/ total aggregate (Vol. %)	Adsorption capacity in 1869 mg/L P-solution (mg/g) (p_i)
	j = 1	j = 2	j = 3	j = 4	
1	350	400	0.33	25	0.15
2	350	450	0.35	50	0.22
3	350	500	0.37	75	0.30
4	400	400	0.35	75	0.29
5	400	450	0.37	25	0.11
6	400	500	0.33	50	0.06
7	450	400	0.37	50	0.02
8	450	450	0.33	75	0.04
9	450	500	0.35	25	0.01
K_{j1}	**0.67**	**0.46**	**0.25**	**0.27**	K = **1.2**
K_{j2}	**0.46**	**0.37**	**0.52**	**0.30**	P = **0.16**
K_{j3}	**0.07**	**0.37**	**0.43**	**0.63**	Q = **0.2628**
Q_j	**0.2218**	**0.1618**	**0.1726**	**0.1866**	
S_j^2	**0.0618**	**0.0018**	**0.0126**	**0.0266**	S_T^2 = **0.1028**

$$Q_j = \frac{1}{m}\sum_{l=1}^{r} K_{jl}^2 \tag{11}$$

$$S_j^2 = Q_j - P \tag{12}$$

$$S_T^2 = \sum_j S_j^2 \tag{13}$$

where, n is the number of experiments; r is the level of each factor; m is the number of occurrences of each level; the values of the n, r and m in this study are 9, 3 and 3, respectively; K_{jl} is the sum of the test results (P_i in Table 9) of the corresponding factor level l ($l = 1,2,3,\cdots,r$) in the column j; P and Q are an intermediate value to facilitate calculation of S_j^2 and S_T^2; S_j^2 is the sum of squares for each factor in the column j; S_T^2 is the sum of squares for total deviations.

Considering the orthogonal table L9 (3^4) is completely filled in this study, the sand has no significant effect on the P-adsorption capacity, with the smallest sum of squares (S_j^2) than other factors (cement, W/C and steel slag), thereby it is used as the error group for the further variance analysis. The variance analysis results are shown in Table 10. As expected, cement and steel slag content have significant effects on the P-adsorption capacity, especially the cement, the water-cement ratio has no significant effect on the adsorption capacity. According to the deviation calculation results (Table 9) and the P-adsorption results, sample No.3 (cement: 350 kg/m^3, sand: 500 kg/m^3, W/C:0.37, 1–2 mm steel slag/total aggregate: 75 vol%) shows excellent P-adsorption capacity and P-removal rate, which is recommended as the optimum mix for pervious concrete.

The adsorption capacity is closely related to the concentration of the solution, reaction time and particle size, etc. [11,70]. The particle size has a significant effect on P-removal efficiency, smaller particle size will release more calcium ions and hydroxide ions to combine with phosphate [71]. The concrete powder has a good P-removal ability of 4.3 mg/g [72]. The pervious concrete with high void and small-sized aggregates has superior P-removal ability due to the large specific surface area [36]. The permeable pavement made of expanded shale aggregate can reduce the P-concentration from 0.22 mg/L to 0.037 mg/L by simulated storm test [4]. The pervious concrete treated with TiO_2 has a purification efficiency of nearly 90% for P removal, with an initial concentration of 1000 mg/L [13]. In this study, the high-concentration P solution (1869 mg/L and 2898 mg/L) and the concrete blocks with a particle mass of 144–178.8 g are used for the P-adsorption test, thereby the P-removal ability of pervious concrete blocks is acceptable.

(2) Effects of cycles on P-adsorption performance.

The adsorption performance of the adsorptive material will gradually decrease after long-term application. The effects of adsorption cycles on P-adsorption capacity and P-removal rate are evaluated and the results are presented in Fig. 16. With the increase in the adsorption cycles, the P-adsorption capacity and P-removal rate of all pervious concrete increases, especially for samples 3 and 4. When the adsorption cycles increase from 1 to 5, the P-adsorption capacity of sample 3 increases from 0.3 mg/g to 0.61 mg/g, and the P-removal rate increases from 15.4% to 31.1%. This indicates that enough calcium ions are released from the pervious concrete for the chemisorption process of Ca-P precipitates, and the adsorption cycles do not reduce the adsorption capacity.

All adsorptive materials will reach saturation at a certain moment. Because only 5 cycles are used for the adsorption test, no saturaton point is observed in this study, more adsorptive cycles need to be carried out for determining the saturation cycles. Moreover, the methods for extending the service life of the pervious concrete after pollutant saturation should be considered in future work, for example, to collect absorbed phosphorus used as fertilizer for plants [73,74] or cultivate microbial communities in micropores structure of pervious concrete to decompose absorbed organic matter [8].

Table 10
Variance analysis of dependent variable of P-adsorption capacity.

Source of variance	Sum of squares	Degree of free	Mean square	F value	Significance
Cement	0.0618	2	0.0309	34.33	*
W/C	0.0126	2	0.0063	7.00	
Steel slag	0.0266	2	0.0133	14.78	(*)
Error	0.0018	2	0.0009		
Total (S_T^2)	0.1028	8			

Notes: The symbols * and (*) represent the significance results under the condition of the significance level of α = 0.10 and 0.05, respectively, and the corresponding critical F values are 9.00 and 19.00, respectively.

4.2.4. Durability

The mass loss of the pervious concrete during the freeze–thaw cycles are presented in Fig. 17a. The mass loss of all concretes is relatively low, except for sample 1. At the 42 freeze–thaw cycles, the mass loss of sample 1 is 2.9%, and the mass loss of other samples series varies from 0.8 to 1.6%. The freeze–thaw damage mainly occurs on the surface of the concrete and the four corners, which is manifested by the peeling of aggregate particles from the concrete surface (Fig. 17b). Compared to the freeze–thaw resistance results of the first part of this study, the freeze–thaw characteristics of pervious concrete have been significantly improved through the optimized mix design. Although samples 5 and 6 show the best freeze–thaw resistance, the P-adsorption capacity and removal rate are relatively low, compared to sample 3 (Fig. 15). Considering the high P-adsorption capacity and suitable strength and durability of sample 3, it is recommended as the optimum mix for pervious concrete.

5. Conclusions

In order to improve the adsorption performance, mechanical properties and durability of pervious concrete, a two-sized aggregate mix, containing steel slag (1–2 mm) and basalt (2–5 mm) is proposed for pervious concrete in this study. The effects of the volumetric substitution ratio (12.5 %, 25.0%, 37.5% and 50%) of steel slag on the physical and mechanical properties, phosphorus (P) adsorption performance and freeze–thaw resistance of pervious concrete are investigated. The optimum mix design of two-sized aggregate pervious concrete is obtained based on the orthogonal test results. The detailed conclusions are as follows:

(1) When the pervious concrete contains 50% steel slag (1–2 mm), the compressive strength and flexural strength of the pervious concrete are increased by 150.8% and 130.7%, respectively, and the mass loss of freeze–thaw cycles decreases by 73.7%, compared to the control concrete. This is attributed to the fact that small-sized steel slag fills the pores between the aggregates and gradually reduces the porosity and permeability, which is beneficial for improving the mechanical strength and freeze–thaw resistance of pervious concrete.
(2) Two-sized aggregate pervious concrete in this study has an excellent P-adsorption capacity, all P is removed from the aqueous solution because the calcium (Ca^{2+}) ion and hydroxide (OH^-) ion released from the pervious concrete react with the phosphate to form Ca-P precipitates. Moreover, the harmful elements (Cr, Sr and V, etc.) leached from the pervious concrete are far lower than the maximum limit value for building materials, confirming no environmental risk.
(3) Orthogonal test results show that cement and steel slag are the main factors affecting the adsorption performance of pervious concrete. Sample 3 (cement: 350 kg/m^3, sand: 500 kg/m^3, W/C: 0.37, 1–2 mm steel slag: 1385.8 kg/m^3 and 2–5 mm basalt: 361.3 kg/m^3) shows excellent adsorption capacity for high-concentration P-removal, which can be used as the optimum

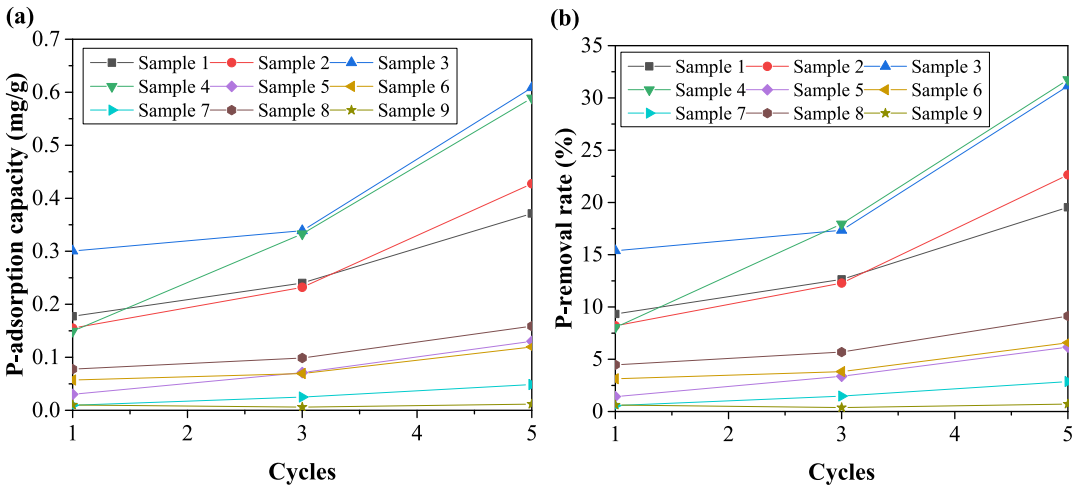

Fig. 16. Effects of cycles on P-adsorption capacity and P-removal rate of pervious concrete.

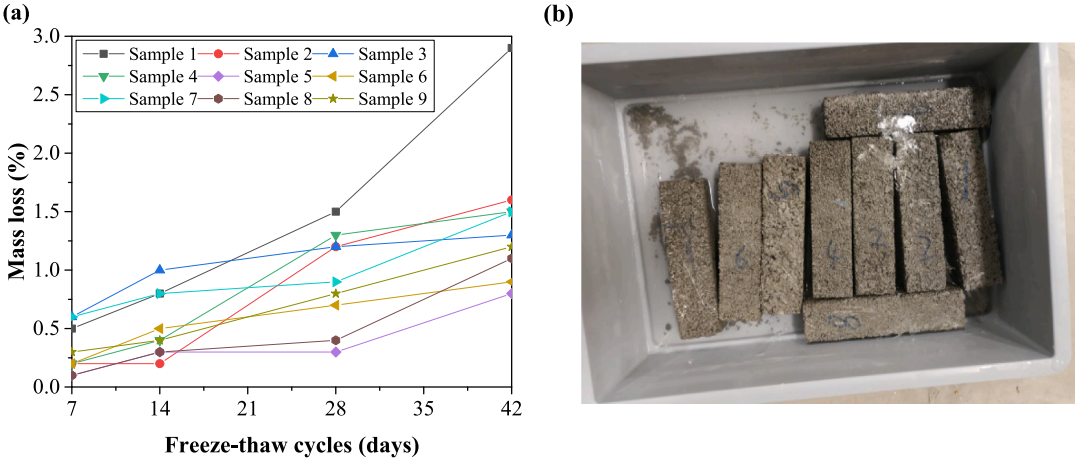

Fig. 17. (a) Mass loss of pervious concrete and (b) Changes in the concrete surface after 42 freeze–thaw cycles.

mix for two-sized aggregate pervious concrete. Moreover, when the cycle increases from 1 to 5, the P-adsorption capacity of sample 3 increases from 0.3 mg/g to 0.61 mg/g, and the P-removal rate increases from 15.4% to 31.1%.

CRediT authorship contribution statement

Fan Wu: Methodology, Investigation, Data curation, Formal analysis, Validation, Funding acquisition, Writing – original draft. **Qingliang Yu:** Conceptualization, Supervision, Project administration, Funding acquisition, Writing – review & editing. **H.J.H. Brouwers:** Supervision, Funding acquisition, Writing – review & editing.

Declaration of Competing Interest

The authors declare that they have no known competing financial interests or personal relationships that could have appeared to influence the work reported in this paper.

Acknowledgements

This work is funded by the National Natural Science Foundation of China (52108358, 52178246), Special Research Assistant Project of the Chinese Academy of Sciences (2021000036), China Postdoctoral Science Foundation (2021M693110) and Eindhoven University of Technology. The authors gratefully thank Ing. Anneke Delsing for the chemical test and analysis, Dr. P. Spiesz from ENCI (The Netherlands) and Prof. dr. S.R. van der Laan from TATA Steel (The Netherlands) for the materials supply.

References

[1] V. Ducman, L. Korat, I. Netinger, I. Barišic, Draining capability of single-sized pervious concrete, Constr. Build. Mater. 169 (2018) 252–260, https://doi.org/10.1016/j.conbuildmat.2018.03.037.
[2] K. Ćosić, L. Korat, V. Ducman, I. Netinger, Influence of aggregate type and size on properties of pervious concrete, Constr. Build. Mater. 78 (2015) 69–76, https://doi.org/10.1016/j.conbuildmat.2014.12.073.
[3] M. Carsana, F. Tittarelli, L. Bertolini, Use of no-fines concrete as a building material: Strength, durability properties and corrosion protection of embedded steel, Cem. Concr. Res. 48 (2013) 64–73, https://doi.org/10.1016/j.cemconres.2013.02.006.
[4] T.K. Ostrom, A.P. Davis, Evaluation of an enhanced treatment media and permeable pavement base to remove stormwater nitrogen, phosphorus, and metals under simulated rainfall, Water Res. 166 (2019) 115071, https://doi.org/10.1016/j.watres.2019.115071.
[5] S. Harada, M. Yanbe, Adsorption by and artificial release of zinc and lead from porous concrete for recycling of adsorbed zinc and lead and of porous concrete to reduce urban non-point heavy metal runoff, Chemosphere. 197 (2018) 451–456, https://doi.org/10.1016/j.chemosphere.2018.01.044.
[6] R.R. Holmes, M.L. Hart, J.T. Kevern, Heavy metal removal capacity of individual components of permeable reactive concrete, J. Contam. Hydrol. 196 (2017) 52–61, https://doi.org/10.1016/j.jconhyd.2016.12.005.

[7] S. Kang, J. Lee, S.M. Park, D.S. Alessi, K. Baek, Adsorption characteristics of cesium onto calcium-silicate-hydrate in concrete powder and block, Chemosphere 259 (2020) 127494, https://doi.org/10.1016/j.chemosphere.2020.127494.
[8] L. Liu, J. Ji, Y. Guo, J. Chen, Use of ecological concrete for nutrient removal in coastal sediment and its effects on sediment microbial communities, Mar. Pollut. Bull. 162 (2021) 111911, https://doi.org/10.1016/j.marpolbul.2020.111911.
[9] J.H. Park, J.J. Wang, S.H. Kim, J.S. Cho, S.W. Kang, R.D. Delaune, D.C. Seo, Phosphate removal in constructed wetland with rapid cooled basic oxygen furnace slag, Chem. Eng. J. 327 (2017) 713–724, https://doi.org/10.1016/j.cej.2017.06.155.
[10] H. Zhu, T. Yu, D. Wei, X. Wang, T. He, Y. Wu, J. Qi, The adsorption of phosphorus in simulated wastewater by immersing and annealing modified attapulgite, Res. Environ. Sci. 31 (2018) 765–773.
[11] F. Wu, Q. Yu, F. Gauvin, H.J.H. Brouwers, C. Liu, Phosphorus removal from aqueous solutions by adsorptive concrete aggregates, J. Clean. Prod. 278 (2021) 123933, https://doi.org/10.1016/j.jclepro.2020.123933.
[12] A.R. Lori, A. Hassani, R. Sedghi, Investigating the mechanical and hydraulic characteristics of pervious concrete containing copper slag as coarse aggregate, Constr. Build. Mater. 197 (2019) 130–142, https://doi.org/10.1016/j.conbuildmat.2018.11.230.
[13] X. Liang, S. Cui, H. Li, A. Abdelhady, H. Wang, H. Zhou, Removal effect on stormwater runoff pollution of porous concrete treated with nanometer titanium dioxide, Transp. Res. Part D Transp. Environ. 73 (2019) 34–45, https://doi.org/10.1016/j.trd.2019.06.001.
[14] E. Teymouri, S.F. Mousavi, H. Karami, S. Farzin, M. Hosseini Kheirabad, Municipal Wastewater pretreatment using porous concrete containing fine-grained mineral adsorbents, J. Water Process Eng. 36 (2020) 101346, https://doi.org/10.1016/j.jwpe.2020.101346.
[15] X. Chen, Y. Guo, S. Ding, H. Zhang, F. Xia, J. Wang, M. Zhou, Utilization of red mud in geopolymer-based pervious concrete with function of adsorption of heavy metal ions, J. Clean. Prod. 207 (2019) 789–800, https://doi.org/10.1016/j.jclepro.2018.09.263.
[16] C. Xie, L. Yuan, H. Tan, Y. Zhang, M. Zhao, Y. Jia, Experimental study on the water purification performance of biochar-modified pervious concrete, Constr. Build. Mater. 285 (2021) 122767, https://doi.org/10.1088/1755-1315/113/1/012126.
[17] L. Mo, S. Yang, B. Huang, L. Xu, S. Feng, M. Deng, Preparation, microstructure and property of carbonated artificial steel slag aggregate used in concrete, Cem. Concr. Compos. 113 (2020) 103715, https://doi.org/10.1016/j.cemconcomp.2020.103715.
[18] Q. Wang, P. Yan, Hydration properties of basic oxygen furnace steel slag, Constr. Build. Mater. 24 (2010) 1134–1140, https://doi.org/10.1016/j.conbuildmat.2009.12.028.
[19] U.S. Geological Survey, Mineral commodity summaries, 2020. https://doi.org/https://doi.org/10.3133/mcs2020.
[20] C. Shi, J. Qian, High performance cementing materials from industrial slags-A review, Resour. Conserv. Recycl. 29 (2000) 195–207, https://doi.org/10.1016/S0921-3449(99)00060-9.
[21] M. Pasetto, A. Baliello, G. Giacomello, E. Pasquini, Sustainable solutions for road pavements: A multi-scale characterization of warm mix asphalts containing steel slags, J. Clean. Prod. 166 (2017) 835–843, https://doi.org/10.1016/j.jclepro.2017.07.212.
[22] E.K. Anastasiou, A. Liapis, M. Papachristoforou, Life cycle assessment of concrete products for special applications containing EAF slag, Procedia Environ. Sci. 38 (2017) 469–476, https://doi.org/10.1016/j.proenv.2017.03.138.
[23] L. Mo, F. Zhang, M. Deng, F. Jin, A. Al-Tabbaa, A. Wang, Accelerated carbonation and performance of concrete made with steel slag as binding materials and aggregates, Cem. Concr. Compos. 83 (2017) 138–145, https://doi.org/10.1016/j.cemconcomp.2017.07.018.
[24] P.E. Tsakiridis, G.D. Papadimitriou, S. Tsivilis, C. Koroneos, Utilization of steel slag for Portland cement clinker production, J. Hazard. Mater. 152 (2008) 805–811, https://doi.org/10.1016/j.jhazmat.2007.07.093.
[25] H. Li, Z. Tang, N. Li, L. Cui, X. zhong Mao, Mechanism and process study on steel slag enhancement for CO2 capture by seawater, Appl. Energy 276 (2020). https://doi.org/10.1016/j.apenergy.2020.115515.
[26] J.H. Park, S.H. Kim, R.D. Delaune, B.H. Kang, S.W. Kang, J.S. Cho, Y.S. Ok, D. C. Seo, Enhancement of phosphorus removal with near-neutral pH utilizing steel and ferronickel slags for application of constructed wetlands, Ecol. Eng. 95 (2016) 612–621, https://doi.org/10.1016/j.ecoleng.2016.06.052.
[27] K.R. Helyar, D.N. Munns, R.G. Burau, Adsorption of phosphate by gibbsite I. effects of neutral chloride salts of calcium, magnesium, sodium, and potassium, J. Soil Sci. 27 (1976) 307–314.
[28] K.R. Helyar, D.N. Munns, R.G. Burau, Adsorption of phosphate by gibbsite II. formation of a surface complex involving divalent cations, J. Soil Sci. 27 (1976) 315–323.
[29] J.J. Lehr, J.C. Van Wesemael, The influence of neutral salts on the solubility of soil phosphate with special reference to the effect of the nitrates of sodium and calcium, J. Soil Sci. 3 (1952) 125–135.
[30] M. Kayhanian, H. Li, J.T. Harvey, X. Liang, Application of permeable pavements in highways for stormwater runoff management and pollution prevention: California research experiences, Int. J. Transp. Sci. Technol. 8 (2019) 358–372, https://doi.org/10.1016/j.ijtst.2019.01.001.
[31] J. Yang, G. Jiang, Experimental study on properties of pervious concrete pavement materials, Cem. Concr. Res. 33 (2003) 381–386, https://doi.org/10.1016/S0008-8846(02)00966-3.
[32] H. Wang, H. Li, X. Liang, H. Zhou, N. Xie, Z. Dai, Investigation on the mechanical properties and environmental impacts of pervious concrete containing fly ash based on the cement-aggregate ratio, Constr. Build. Mater. 202 (2019) 387–395, https://doi.org/10.1016/j.conbuildmat.2019.01.044.
[33] M.T. de Grazia, L.F.M. Sanchez, R.C.O. Romano, R.G. Pileggi, Investigation of the use of continuous particle packing models (PPMs) on the fresh and hardened properties of low-cement concrete (LCC) systems, Constr. Build. Mater. 195 (2019) 524–536, https://doi.org/10.1016/j.conbuildmat.2018.11.051.
[34] S.H. Chu, C.S. Poon, C.S. Lam, L. Li, Effect of natural and recycled aggregate packing on properties of concrete blocks, Constr. Build. Mater. 278 (2021) 122247, https://doi.org/10.1016/j.conbuildmat.2021.122247.
[35] Reading: Crystal structures with cubic unit cells, (n.d.) Revised 5/3/04. https://www.yumpu.com/en/document/read/19936742/crystal-structures-with-cubic-unit-cells.
[36] S.B. Park, M. Tia, An experimental study on the water-purification properties of porous concrete, Cem. Concr. Res. 34 (2004) 177–184, https://doi.org/10.1016/S0008-8846(03)00223-0.
[37] N. Sebaibi, M. Benzerzour, Y. Sebaibi, N.E. Abriak, Composition of self compacting concrete (SCC) using the compressible packing model, the Chinese method and the European standard, Constr. Build. Mater. 43 (2013) 382–388, https://doi.org/10.1016/j.conbuildmat.2013.02.028.
[38] N.S. Klein, L.A. Lenz, W. Mazer, Influence of the granular skeleton packing density on the static elastic modulus of conventional concretes, Constr. Build. Mater. 242 (2020) 118086, https://doi.org/10.1016/j.conbuildmat.2020.118086.
[39] Z. Dai, H. Li, W. Zhao, X. Wang, H. Wang, H. Zhou, B. Yang, Multi-modified effects of varying admixtures on the mechanical properties of pervious concrete based on optimum design of gradation and cement-aggregate ratio, Constr. Build. Mater. 233 (2020) 117178, https://doi.org/10.1016/j.conbuildmat.2019.117178.
[40] Y. Chen, Q.L. Yu, H.J.H. Brouwers, Acoustic performance and microstructural analysis of bio-based lightweight concrete containing miscanthus, Constr. Build. Mater. 157 (2017) 839–851, https://doi.org/10.1016/j.conbuildmat.2017.09.161.
[41] D.H. Nguyen, M. Boutouil, N. Sebaibi, F. Baraud, L. Leleyter, Durability of pervious concrete using crushed seashells, Constr. Build. Mater. (2017), https://doi.org/10.1016/j.conbuildmat.2016.12.219.
[42] M.S. Sumanasooriya, N. Neithalath, Pore structure features of pervious concretes proportioned for desired porosities and their performance prediction, Cem. Concr. Compos. 33 (2011) 778–787, https://doi.org/10.1016/j.cemconcomp.2011.06.002.
[43] L. Haselbach, C. Poor, J. Tilson, Dissolved zinc and copper retention from stormwater runoff in ordinary Portland cement pervious concrete, Constr. Build. Mater. 53 (2014) 652–657, https://doi.org/10.1016/j.conbuildmat.2013.12.013.
[44] Y. Zhang, H. Li, A. Abdelhady, J. Yang, H. Wang, Effects of specimen shape and size on the permeability and mechanical properties of porous concrete, Constr. Build. Mater. 266 (2021) 121074, https://doi.org/10.1016/j.conbuildmat.2020.121074.
[45] C. Lian, Y. Zhuge, Optimum mix design of enhanced permeable concrete - An experimental investigation, Constr. Build. Mater. 24 (2010) 2664–2671, https://doi.org/10.1016/j.conbuildmat.2010.04.057.
[46] M.S. Sumanasooriya, D.P. Bentz, N. Neithalath, Planar image-based reconstruction of pervious concrete pore structure and permeability prediction, ACI Mater. J. 107 (2010) 413–421.
[47] Z. Wang, D. Zou, T. Liu, A. Zhou, M. Shen, A novel method to predict the mesostructure and performance of pervious concrete, Constr. Build. Mater. 263 (2020) 120117, https://doi.org/10.1016/j.conbuildmat.2020.120117.
[48] W. Yeih, T.C. Fu, J.J. Chang, R. Huang, Properties of pervious concrete made with air-cooling electric arc furnace slag as aggregates, Constr. Build. Mater. 93 (2015) 737–745, https://doi.org/10.1016/j.conbuildmat.2015.05.104.
[49] S. Wang, G. Zhang, B. Wang, M. Wu, Mechanical strengths and durability properties of pervious concretes with blended steel slag and natural aggregate, J. Clean. Prod. 271 (2020) 122590, https://doi.org/10.1016/j.jclepro.2020.122590.
[50] T. Liu, Z. Wang, D. Zou, A. Zhou, J. Du, Strength enhancement of recycled aggregate pervious concrete using a cement paste redistribution method, Cem. Concr. Res. 122 (2019) 72–82, https://doi.org/10.1016/j.cemconres.2019.05.004.
[51] P. Shen, H. Zheng, S. Liu, J.X. Lu, C.S. Poon, Development of high-strength pervious concrete incorporated with high percentages of waste glass, Cem. Concr. Compos. 114 (2020) 103790, https://doi.org/10.1016/j.cemconcomp.2020.103790.
[52] P. Mehrabi, M. Shariati, K. Kabirifar, M. Jarrah, H. Rasekh, N.T. Trung, A. Shariati, S. Jahandari, Effect of pumice powder and nano-clay on the strength and permeability of fiber-reinforced pervious concrete incorporating recycled concrete aggregate, Constr. Build. Mater. 287 (2021) 122652, https://doi.org/10.1016/j.conbuildmat.2021.122652.
[53] G. Xu, W. Shen, X. Huo, Z. Yang, J. Wang, W. Zhang, X. Ji, Investigation on the properties of porous concrete as road base material, Constr. Build. Mater. 158 (2018) 141–148, https://doi.org/10.1016/j.conbuildmat.2017.09.151.
[54] F. Wu, Q. Yu, H.J.H. Brouwers, Phosphorus removal enhancement by porous adsorptive mortar using miscanthus and steel slag for highly adsorptive concrete, Constr. Build. Mater. 295 (2021) 123686, https://doi.org/10.1016/j.conbuildmat.2021.123686.
[55] H. Yin, Y. Yun, Y. Zhang, C. Fan, Phosphate removal from wastewaters by a naturally occurring, calcium-rich sepiolite, J. Hazard. Mater. 198 (2011) 362–369, https://doi.org/10.1016/j.jhazmat.2011.10.072.
[56] A.K. Chandrappa, K.P. Biligiri, Pervious concrete as a sustainable pavement material-Research findings and future prospects: A state-of-the-art review, Constr. Build. Mater. 111 (2016) 262–274, https://doi.org/10.1016/j.conbuildmat.2016.02.054.
[57] Z. Ma, R. Xue, J. shan Li, Y. Zhao, Q. Xue, Z. Chen, Q. Wang, C.S. Poon, Use of thermally modified waste concrete powder for removal of Pb (II) from wastewater:

Effects and mechanism, Environ. Pollut. 277 (2021) 116776. https://doi.org/10.1016/j.envpol.2021.116776.
[58] D.H. Nguyen, M. Boutouil, N. Sebaibi, F. Baraud, L. Leleyter, Durability of pervious concrete using crushed seashells, Constr. Build. Mater. 135 (2017) 137–150, https://doi.org/10.1016/j.conbuildmat.2016.12.219.
[59] Dutch Soil Quality Decree, Maximum composition and emission values for building materials, Regeling Bodemkwaliteit. (2015).
[60] M.A. González-Ortega, S.H.P. Cavalaro, G. Rodríguez de Sensale, A. Aguado, Durability of concrete with electric arc furnace slag aggregate, Constr. Build. Mater. 217 (2019) 543–556, https://doi.org/10.1016/j.conbuildmat.2019.05.082.
[61] F. Wu, Q. Yu, C. Liu, Durability of thermal insulating bio-based lightweight concrete: Understanding of heat treatment on bio-aggregates, Constr. Build. Mater. 269 (2021) 121800, https://doi.org/10.1016/j.conbuildmat.2020.121800.
[62] B. Pang, Z. Zhou, X. Cheng, P. Du, H. Xu, ITZ properties of concrete with carbonated steel slag aggregate in salty freeze-thaw environment, Constr. Build. Mater. 114 (2016) 162–171, https://doi.org/10.1016/j.conbuildmat.2016.03.168.
[63] F. Gong, S. Jacobsen, Modeling of water transport in highly saturated concrete with wet surface during freeze/thaw, Cem. Concr. Res. 115 (2019) 294–307, https://doi.org/10.1016/j.cemconres.2018.08.013.
[64] O. Coussy, P.J.M. Monteiro, Poroelastic model for concrete exposed to freezing temperatures, Cem. Concr. Res. 38 (2008) 40–48, https://doi.org/10.1016/j.cemconres.2007.06.006.
[65] Z. Sun, G.W. Scherer, Effect of air voids on salt scaling and internal freezing, Cem. Concr. Res. 40 (2010) 260–270, https://doi.org/10.1016/j.cemconres.2009.09.027.
[66] M. Sun, D. Xin, C. Zou, Damage evolution and plasticity development of concrete materials subjected to freeze-thaw during the load process, Mech. Mater. 139 (2019), https://doi.org/10.1016/j.mechmat.2019.103192.
[67] M. Vancura, K. MacDonald, L. Khazanovich, Microscopic analysis of paste and aggregate distresses in pervious concrete in a wet, hard freeze climate, Cem. Concr. Compos. 33 (2011) 1080–1085, https://doi.org/10.1016/j.cemconcomp.2011.05.011.
[68] X. Nan, Z. Wang, J. Hou, Y. Tong, B. Li, Clogging mechanism of pervious concrete: From experiments to CFD-DEM simulations, Constr. Build. Mater. 270 (2021) 1–11, https://doi.org/10.1016/j.conbuildmat.2020.121422.
[69] H. Yang, F. Wei, K. Hu, Determination of the maximum packing fraction for calculating slurry viscosity of debris flow, Mt. Res. 36 (2018) 382–390.
[70] M.T. Vu, L.N. Nguyen, M.A. Hasan Johir, H.H. Ngo, C. Skidmore, A. Fontana, B. Galway, H. Bustamante, L.D. Nghiem, Phosphorus removal from aqueous solution by steel making slag – Mechanisms and performance optimisation, J. Clean. Prod. 284 (2021) 124753. https://doi.org/10.1016/j.jclepro.2020.124753.
[71] D. Liu, H. Zhu, K. Wu, F. Wang, X. Zhao, Q. Liao, Understanding the effect of particle size of waste concrete powder on phosphorus removal efficiency, Constr. Build. Mater. 236 (2020) 117526, https://doi.org/10.1016/j.conbuildmat.2019.117526.
[72] G.M. Kim, J.G. Jang, H.R. Khalid, H.K. Lee, Water purification characteristics of pervious concrete fabricated with CSA cement and bottom ash aggregates, Constr. Build. Mater. 136 (2017) 1–8, https://doi.org/10.1016/j.conbuildmat.2017.01.020.
[73] V. Arenas-Montaño, O. Fenton, B. Moore, M.G. Healy, Evaluation of the fertiliser replacement value of phosphorus-saturated filter media, J. Clean. Prod. 291 (2021), https://doi.org/10.1016/j.jclepro.2021.125943.
[74] K. Haarstad, J. Bavor, Phosphorus Recycling from Wastes, J. Environ. Prot. (Irvine, Calif) 08 (2017) 831–843, https://doi.org/10.4236/jep.2017.88052.